# Supplemental material for optically addressing single rare-earth ions in a nanophotonic cavity

Tian Zhong,[1,2,3,*] Jonathan M. Kindem,[1,2] John G. Bartholomew,[1,2] Jake Rochman,[1,2] Ioana Craiciu,[1,2] Varun Verma,[4] Sae Woo Nam,[4] Francesco Marsili,[5] Matthew D. Shaw,[5] and Andrei Faraon[1,2,†]

[1]*Kavli Nanoscience Institute and Thomas J. Watson, Sr., Laboratory of Applied Physics, California Institute of Technology, Pasadena, California 91125, USA.*
[2]*Institute for Quantum Information and Matter, California Institute of Technology, Pasadena, California 91125, USA.*
[3]*Institute for Molecular Engineering, University of Chicago, Chicago, IL 60637, USA.*
[4]*National Institute of Standards and Technology, 325 Broadway, MC 815.04, Boulder, Colorado 80305, USA*
[5]*Jet Propulsion Laboratory, California Institute of Technology, 4800 Oak Grove Drive, Pasadena, California 91109, USA*

(Dated: October 8, 2018)

## DETAILS ON THE EXPERIMENTAL SETUP

Figure S1 illustrates the experimental setup with more details. The $Nd^{3+}$:$YVO_4$ sample crystal was soldered with indium onto a copper plate that was mounted on top of a 3-axis nanopositioner, and was thermally connected to the 20 mK base plate of the dilution refrigerator. Cavity tuning was realized by gas condensation using $N_2$ gas. The gas tube (brown line in Fig. S1) was thermally anchored to the 3.8 K stage. When performing gas tuning, a heater on the gas tube heats it up to >30 K to allow gas to flow through. The heater was turned off after tuning. This configuration was used to minimize the heat load generated by the tube, allowing the lowest possible temperature at the sample.

**Fiber-waveguide coupling efficiency** The coupling to the waveguide was realized by a 45°-angled cut into the $YVO_4$ substrate [1]. This angled cut allows the vertically focused beam (from a fiber) to be total internally reflected into the nanobeam waveguide. The aspherical doublet has an effective focal length of 10.5 mm on the fiber side and 2.9 mm on the sample side (Fig.S1). The coupling was optimized by fine scanning the focal spot on the sample surface using the nanopositioner and looking for the cavity resonance on a spectrometer. The overall fiber-waveguide coupling efficiency was characterized by measuring the reflection of a pulse far off resonance with the cavity (i.e. in the photonic bandgap). The pulse propagated from point 1 (marked in Fig.S1) to 2, 3, and was reflected back to 2, then 4. The transmission efficiency from 1 to 2 (64.1%), and from 2-4 (51.7%) were directly measured. The only unknown was the coupling efficiency from 2 to 3. This coupling efficiency could be uniquely determined from the total pulse reflection, and was found to be 19%.

**Photon collection efficiency** For each photon emitted by an ion into the cavity, the probability of that photon to be transmitted to the coupling waveguide was $\kappa_{in}/\kappa$=45%. The photon then propagated from 3 to 2 (19% waveguide-fiber coupling), and from 2 to 4 (79.9% transmission through all fiber slices/connectors and 64.7% transmission through the optical circulator), and was finally detected by the 82%-efficient superconducting nanowire detector. Thus, the overall collection efficiency for a cavity photon was $0.45\times0.19\times0.80\times0.65\times0.82 = 3.6\%$. To improve this efficiency, further refinement in fabrication is needed to achieve a highly over-coupled cavity with $\kappa_{in}/\kappa$ >80%, which should be within reach since we have achieved symmetric two-sided cavities of Q as high as 20,000 [2]. Furthermore, the use of tapered fiber-waveguide coupling could improve the fiber-to-device coupling to 97% [3]. These combined with lower loss fiber components could increase the overall efficiency to ∼70%.

**Cavity mean photon number** To obtain the cavity mean photon number in Fig.3, we first calculate the peak power of the excitation pulse in the waveguide i.e. $P_{in}$ with knowledge of the transmission from 1 to 2 and the coupling efficiency from 2 to 3. The cavity mean photon number was $\bar{n} = 4P_{in}\kappa_{in}/\hbar\omega_0\kappa^2$, where $\kappa_{in} = 2\pi\times40$ GHz was the cavity in-coupling rate, $\kappa = 2\pi\times90$ GHz was the total cavity decay rate, and $\omega_0$ is the photon frequency.

### Optical properties of $Nd^{3+}$ in $YVO_4$ and Purcell factor

The absorption area $\int\alpha(\nu)d\nu$ for the $^4I_{9/2}(Z_1) \leftrightarrow {}^4F_{3/2}(Y_1)$ optical transition in a 10 ppm $Nd^{3+}$:$YVO_4$ sample was measured in zero magnetic field with E ∥ c by Sun *et al.* [4] to be 3.4 $cm^{-1}$ $cm^{-1}$ = 102 GHz $cm^{-1}$. Because the electric dipole transition is heavily π-polarized, we can calculate the transition oscillator strength from the absorption area $\int\alpha(\nu)d\nu$ using [5, 6]

$$f = 4\pi\epsilon_0\frac{m_e c}{\pi e^2}\frac{1}{N}\frac{n}{{\chi_L}^2}\int\alpha(\nu)d\nu \ , \qquad (1)$$

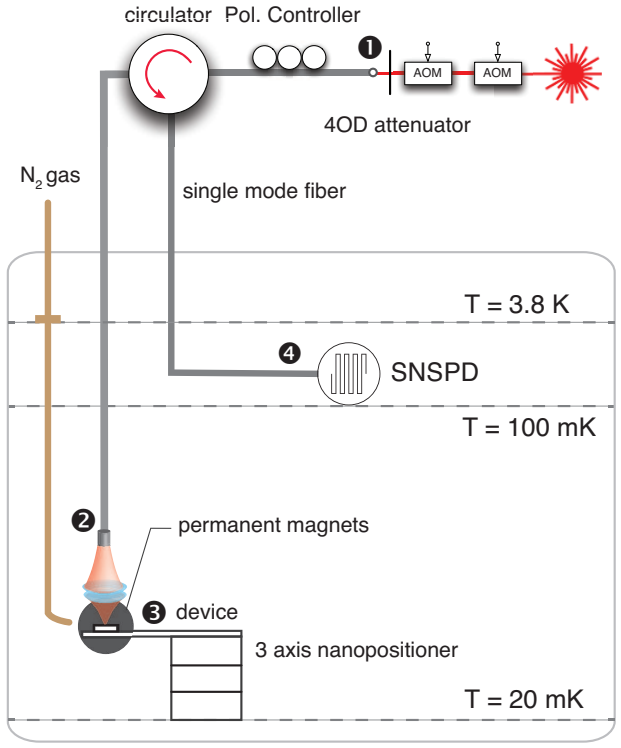


FIG. S1: Details of the experimental setup. SNSPD: superconducting nanowire single photon detector.

where $\epsilon_0$ is the vacuum permittivity, $m_e$ is the mass of the electron, $e$ is the charge on the electron, $c$ is the speed of light, $N$ is the number density, $\chi_L$ is the local field correction, $n$ is the refractive index, and $\alpha(\nu)$ is the absorption coefficient as a function of frequency $\nu$.

For the 10 ppm $Nd^{3+}$:$YVO_4$ crystal measured by Sun *et al.* [4], $N = 1.24 \times 10^{23}$ m$^{-3}$ and $n = 2.1785$ for light polarized along the $c$-axis of the crystal. The local field correction factor $\chi_L$ usually takes one of two forms in the literature, depending on whether the virtual cavity or real cavity model is used [7–10]:

$$\chi_L^{(V)} = \frac{n^2+2}{3} \quad , \tag{2}$$

is the virtual cavity model, and

$$\chi_L^{(R)} = \frac{3n^2}{2n^2+1} \quad , \tag{3}$$

is the real cavity model correction.

Both the virtual and real cavity models are approximations to the full local field correction in that they assume that the field due to the polarization of atoms nearby in the lattice is zero [10]. The real cavity model has been shown to be suitable for substitutional ions [11] including rare-earth ions in crystalline hosts [7]. In this work, the predictions based on the real cavity model are more consistent with our current knowledge of material and experimental results.

We note that there is inconsistency in the literature regarding oscillator strengths and dipole moments of 4f - 4f transitions for rare-earth ions in crystals because values and expressions are not always explicit as to which local field correction, if any, is assumed. Here we detail our derivations to make it clear the assumptions we have made and how that impacts the theoretical predictions.

When assuming the real cavity model for the local field correction, from Eq. 1 we calculate an oscillator strength $f = 3.7 \times 10^{-5}$. For the applied field of 390 mT along the a-axis we expect optical transitions 2 and 3 to be forbidden. In this case, transitions 1 and 4 each have an oscillator strength $f = 3.7 \times 10^{-5}$.

The radiative lifetime $T_{rad}$ is related to the oscillator strength $f$ by [5, 6]

$$\frac{1}{T_{rad}} = \frac{2\pi e^2}{\epsilon_0 m_e c}\left(\frac{3n^2}{2n^2+1}\right)^2 \frac{1}{n}\frac{n^2}{\lambda^2}\frac{f}{3} \quad , \tag{4}$$

which gives a value of $T_{rad} = 237$ $\mu$s. Given the lifetime of the $^4F_{3/2}(Y_1)$ state measured by fluorescence was $T_1 = 90$ $\mu$s, the branching ratio of emission to the $^4I_{9/2}(Z_1)$ state is $\beta = 0.38$.

The transition dipole moment $\mu$ is related to the oscillator strength $f$ by [5, 6]

$$\mu = \sqrt{\frac{\hbar e^2 f}{2 m_e \omega}} \quad , \tag{5}$$

where $\omega = 2\pi c/\lambda$ is the frequency $^4I_{9/2}(Z_1) \leftrightarrow {}^4F_{3/2}(Y_1)$ optical transition. Equation 5 differs from the expressions relating $\mu$ to $f$ in [10]. This is because in [10] no field corrections are assumed in relating $f$ to $\int \alpha(\nu) d\nu$. Using Equation 5, we calculate a dipole moment $\mu = 1.59 \times 10^{-31}$ C·m.

Given $g_0$ and the cavity energy decay rate $\kappa = 2\pi \times 90$ GHz, the lifetime of the $Nd^{3+}$ ion in the cavity is given by

$$T_{cav} = \left(\frac{4g_0^2}{\kappa} + \frac{1-\beta}{T_1}\right)^{-1} \quad . \tag{6}$$

Therefore, the predicted $T_{cav} = 1.25$ $\mu$s. The Purcell enhancement factor of the resonant transition is derived to be $4g_0^2 T_{rad}/\kappa = 189$.

## PHOTON ECHO MEASUREMENTS

Two pulse photon echo measurements were performed on an ensemble of ions in the cavity near the center of inhomogeneous distribution (e.g. line 1). The cavity resonance was tuned to different frequencies using a gas condensation technique to obtain homogeneous linewidths of ions at varying Purcell enhancement conditions. Fig.S2 plots the photon echo decays at ensemble-cavity detuning

of $\delta$ ~22 and ~50 GHz. Oscillations in the echo intensities correspond to syperhyperfine interactions between Nd spins and Y nuclear spins [12] at 740 kHz, which agree with the beat frequency observed in the Ramsey interference fringes. Note that the period of the oscillations appears to be twice long in the Ramsey fringes than in the echo decays, because the photon echo is emitted after twice the delay between two pulses. The $T_2$ were fitted from the linear section of the decay, which started after approximately 4 $\mu$s.

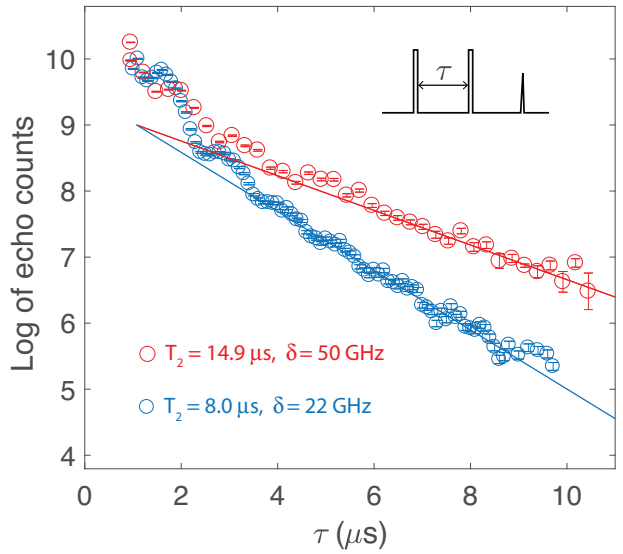


FIG. S2: Photon echoes on sub-ensembles of Nd ions coupled to the cavity at different cavity-ensemble detunings. The oscillations evident in the initial echo intensity decays were due to superhyperfine couplings between Nd and Y spins. $T_2$ was fitted from the linear decay sections (>4 $\mu$s). A difference in $T_2$ at varying detunings reflects the change of radiative decay rates (i.e.$T_1$) under different Purcell enhancement factors.

## MODELLING SUPERHYPERFINE COUPLINGS

The superhyperfine interaction is between an electronic spin (Nd in this case) and a neighbouring ligand nuclear spin (yttrium or vanadium). This interaction has been studied in the literature and was typically orders of magnitude weaker than the rare-earth electronic Zeeman interactions (the gyromagnetic ratio of $Nd^{3+}$ is 3.9-33 GHz/T). As a result, the associated Hamiltonian can be treated as a perturbation to the electronic Zeeman coupling of $Nd^{3+}$ under external applied magnetic field [13].

$$H' = -\mu_Y \cdot \left( \mathbf{B} - \frac{\mu_0}{4\pi} \left[ \frac{\langle \mu^{Nd} \rangle}{r^3} - 3 \frac{(\langle \mu^{Nd} \rangle \cdot \mathbf{r}) \cdot \mathbf{r}}{r^5} \right] \right) \quad (7)$$

where $\mu_Y$ is the $Y^{3+}$ nuclear spin magnetic moment, $\mathbf{B}$ the externally applied magnetic field, $\mu^{Nd}$ the $Nd^{3+}$ electronic spin and $\mathbf{r}$ the vector connecting two spins. The superhyperfine coupling at zero field - the terms in Eq. (7) that are not dependent on $\mathbf{B}$ - causes each of the Zeeman levels (both ground and excited) to split into a nuclear doublet. Such splitting can be readily calculated from the electronic magnetic dipole moment from the known anisotropic g-factors of Nd. As the applied field increases, eventually the term $-\mu_Y \cdot \mathbf{B}$ dominates over other terms and the splitting becomes approximately linear with $\mathbf{B}$. Thus, in high fields, the superhyperfine splitting strongly depends on the gyromagnetic ratios of specific ligand nuclear spins. For yttrium it is 2.1 MHz/T. For vanadium it is 11.2 MHz/T. At B = 390 mT along a-axis, the expected superhyperfine splitting of each of the Zeeman branches can be estimated based on atomic coordinates of the yttrium or vanadium ions surrounding the Nd center.

For Nd-Y coupling, there are 4 nearest neighbour Y ions at equal distance of 3.9Å from each Nd ion. The zero-field superhyperfine splitting is calculated to be ~80 kHz and ~30 kHz for the optical ground and excited levels, respectively. With an applied field of 390 mT along a-axis, the total splitting from Eq. (7) gives $\Delta_g$ ~740 kHz and $\Delta_e$ ~790 kHz for ground and excited levels.

For Nd-V coupling, the nearest distance between them is 3.14 Å. Since vanadium has 7/2 spins, there are a total of 8 superhyperfine sublevels. The splittings between those levels at 390 mT field ranges from ~4 -30 MHz. Given that the optical excitation pulse only has a bandwidth of 2 MHz, it is unlikely that multiple Nd-V superhyperfine sublevels were excited.

The envelope modulation in Fig. 3(b) can be modelled after derivations in [14], which include beatings at frequencies $\Delta_e$, $\Delta_g$, $(\Delta_e - \Delta_g)$ and $(\Delta_e + \Delta_g)$, with their relative strengths dependent on the degree of spin mixing. Due to limited sampling and likely over-simplification of the model, the experimental data (black) in Fig. 3(b) cannot be fitted well with a known analytical form. Instead, an empirical fit (red) was used to identify the dominant beat frequency. The best fit gives 740 kHz, which is in general agreement with the $\Delta_e$, $\Delta_g$ calculated above. We therefore infer that the observed beating was likely originated from the Nd-Y superhyperfine interaction but unlikely from Nd-V couplings. The latter is expected to give a splitting >4 MHz. The Nd-V superhyperfine coupling was indeed reported in [15] in the same $Nd^{3+}$:$YVO_4$ material to be about 5 MHz at 0.3 T field.

## OPTICAL DEPHASING IN $Nd^{3+}$:$YVO_4$

Possible contributions to the optical dephasing $\gamma^*$=9.7 kHz include superhyperfine coupling between Nd spins and yttrium/vanadium nuclear spins, the Nd spin flip-flops, direct phonon couplings, and other higher order processes. Here we discuss contributions from two po-

tentially dominant mechanisms.

**Superhyperfine interaction** The experimental condition in the current work closely reassembles that in [4] in which optical $T_2$ for a 10 ppm doped $Nd^{3+}$:$YVO_4$ sample was measured at varying magnetic field applied along the a-axis of the crystal. It was found in [4] that with a field greater than 1.5 T, the $T_2$ of 27 $\mu$s became limited by the Nd-Vanadium superhyperfine interaction. The corresponding dephasing rate could be calculated from $1/(\pi T_2)$ - $1/(2\pi T_1)$ = 10.0 kHz, which was very close to the dephasing rate measured here. We thus expect that the superhyperfine interactions contribute substantially to the measured $\gamma^*$. Based on the spin interaction models in [16], we could numerically estimate the broadenings due to Nd-Y and Nd-V interactions to be 34 and 14 kHz, respectively; these values are in order-of-magnitude agreement with the measurement.

**Nd spin flip-flops** Dephasing due to the Nd spin flip-flops is a function of the Nd doping concentration and temperature. To better understand this process, we measured optical $T_2$ times in both the 50 ppm doped (the same crystal on which the devices were fabricated) and a nominally undoped $YVO_4$ crystal. From the absorption spectroscopy and secondary ion mass spectroscopy (SIMS), we estimated the doping concentration of Nd to be ≈0.2 ppm in the undoped $YVO_4$. Therefore, the dephasing owing to spin flip-flops is expected to be relatively small in that sample. Both crystals were soldered to a common sample holder. With the same magnetic field configuration as in the main text, the ground level splitting was $\mu_B g_\perp \mathbf{B}$=12.88 GHz where $g_\perp$=2.36 is the ground state g-factor [17, 18], and $\mathbf{B}$ = 0.39 T. We then used the ratio between the absorptions of two Zeeman transitions to calibrate the crystal temperature. When both crystals were at ∼500 mK, we measured a $T_2^{\mathrm{doped}}$ = 25.4 $\mu$s and $T_2^{\mathrm{undoped}}$ = 27.0 $\mu$s in 50 ppm doped and undoped $YVO_4$ crystals, respectively. The difference in linewidths, which amounts to <1 kHz, serves as an upper bound on dephasing due to Nd spin flip-flops at 500 mK.

Using the models put forth by [16, 19], the optical dephasing due to Nd-Nd spin flip-flops can be estimated from a Lorentzian spectral diffusion model as $1/\pi T_M$ [19] where

$$T_M = \frac{2\Gamma_0}{\Gamma_{\mathrm{SD}} R}\left(-1+\sqrt{1+\frac{\Gamma_{\mathrm{SD}} R}{\pi\Gamma_0^2}}\right), \qquad (8)$$

where $\Gamma_{\mathrm{SD}}$ is the Nd magnetic dipolar interaction,

$$\Gamma_{\mathrm{SD}} = \frac{\pi\mu_0|g_g - g_e| g_g \mu_B^2 n_{\mathrm{Nd}}}{9\sqrt{3}\hbar} sech^2\left(\frac{g_g \mu_B B}{2kT}\right) \qquad (9)$$

and $R = 1/T_1^{spin}$. Using $n_{\mathrm{Nd}} = 6.3\times10^{23}$ m$^{-3}$ as the Nd concentration at 50 ppm doping, and Nd spin $T_1^{spin}$=98 ms measured from spectral holeburning at 500 mK, we predict a corresponding optical dephasing to be 30 Hz [19]. This implies that our measurement is dominated by other interactions, such as the superhyperfine interaction.

* Electronic address: tzh@uchicago.edu
† Electronic address: faraon@caltech.edu

[1] T. Zhong, *et al. Science* **357,** 1392-1395 (2017).
[2] T. Zhong, J. Rochman, J. M. Kindem, E. Miyazono, and A. Faraon, *Opt. Express* **24,** 536-544 (2016).
[3] T. G. Tiecke, K. P. Nayak, J. D. Thompson, T. Peyronel, N. P. de Leon, V. Vuletić, and M. D. Lukin, *Optica* **2,** 70-75 (2015).
[4] Y. Sun, C. W. Thiel, R. L. Cone, R. W. Equall, and R. L. Hutcheson, *J. Lumin.* **98,** 281-287 (2002).
[5] B. Di Bartolo, Optical interactions in solids (Wiley, New York, 1968).
[6] B. Henderson and G. Imbush, Optical spectroscopy of inorganic solids (Oxford University Press, 2006).
[7] K. Dolgaleva, and R. W. Boyd, Adv. Opt. Photon. 4, 1-77 (2012).
[8] H. T. Dung, S. Y. Buhmann, and D.-G. Welsch, Phys. Rev. A 74, 023803 (2006).
[9] D. L. McAuslan, J. J. Longdell, and M. J. Sellars, Phys. Rev. A 80, 6 062307 (2009).
[10] M. F. Reid, in *Spectroscopic Properties of Rare Earths in Optical Materials*, edited by G. Liu and B. Jacquier (Springer Berlin Heidelberg, 2005).
[11] P. de Vries, and A. Lagendijk, Phys. Rev. Lett., 81, 7, 1381-1384 (1998).
[12] I. Usmani, M. Afzelius, H. de Riedmatten and N. Gisin, *Nature Commun.* **1,** 12 (2010).
[13] B. Car, L. Veissier, A. Louchet-Chauvet, J.-L. Le Gouët and T. Chanelière, *Phys. Rev. Lett.* **120,** 197401 (2018).
[14] W. B. Mims, *Phys. Rev. B* **5,** 2409 (1972).
[15] H. de Riedmatten, M. Afzelius, M. U. Staudt, C. Simon and N Gisin, *Nature* **456,** 773-777 (2008).
[16] T. Böttger, C. W. Thiel, Y. Sun, and R. L. Cone, *Phys. Rev. B* **73,** 075101 (2006)
[17] S. R. Hasting-Simon, *et al. Phys. Rev. B* **77,** 125111 (2008).
[18] M. Afzelius, *et al. J. Luminescence* **130,** 1566-1571 (2010).
[19] T. Böttger, C. W. Thiel, R. L. Cone, and Y. Sun, *Phys. Rev. B* **79,** 115104 (2009)